

Article

Design, Synthesis, and Antiproliferative Activity of Selective Histone Deacetylases 6 Inhibitors Containing a Tetrahydropyridopyrimidine Scaffold

 Bin Wang ^{1,†}, Youcai Liu ^{2,†}, Lejing Zhang ¹, Yajuan Wang ¹, Zhaoxi Li ¹ and Xin Chen ^{3,*} 
¹ Department of Biochemistry and Molecular Biology, Sanquan College of Xinxiang Medical University, Xinxiang 453003, China; wangbin@sqmc.edu.cn (B.W.); lejing.2008.cool@163.com (L.Z.); jjxcz@126.com (Y.W.)

² Experimental Teaching Center of Biology & Basic Medicine, Sanquan College of Xinxiang Medical University, Xinxiang 453003, China; 09513063@sqmc.edu.cn

³ Shaanxi Key Laboratory of Natural Products & Chemical Biology, College of Chemistry & Pharmacy, Northwest A&F University, Xianyang 712100, China

* Correspondence: chenxin1888@nwsuaf.edu.cn; Tel.: +86-029-87092335

[†] The authors contributed equally to this paper.

Abstract: The development of selective histone deacetylase 6 inhibitors (sHDAC6is) is being recognized as a therapeutic approach for cancers. In this paper, we designed a series of novel tetrahydropyridopyrimidine derivatives as sHDAC6 inhibitors. The most potent compound, 8-(2, 4-bis(3-methoxyphenyl)-5, 8-dihydropyrido [3, 4-*d*]pyrimidin-7(6*H*)-yl)-*N*-hydroxy-8-oxooctanamide (**8f**), inhibited HDAC6 with IC₅₀ of 6.4 nM, and showed > 48-fold selectivity over other subtypes. In Western blot assay, **8f** elevated the levels of acetylated α -tubulin in a dose-dependent manner. In vitro, **8f** inhibited RPMI-8226, HL60, and HCT116 tumor cells with IC₅₀ of 2.8, 3.20, and 3.25 μ M, respectively. Moreover, **8f** showed good antiproliferative activity against a panel of tumor cells.

Keywords: HDAC6 inhibitor; tetrahydropyridopyrimidine; antitumor; synthesis; selectivity



Citation: Wang, B.; Liu, Y.; Zhang, L.; Wang, Y.; Li, Z.; Chen, X. Design, Synthesis, and Antiproliferative Activity of Selective Histone Deacetylases 6 Inhibitors Containing a Tetrahydropyridopyrimidine Scaffold. *Molecules* **2023**, *28*, 7323. <https://doi.org/10.3390/molecules28217323>

Academic Editors: Bruno Botta, Shuai Wang and Fen Er Chen

Received: 20 September 2023

Revised: 19 October 2023

Accepted: 27 October 2023

Published: 29 October 2023



Copyright: © 2023 by the authors. Licensee MDPI, Basel, Switzerland. This article is an open access article distributed under the terms and conditions of the Creative Commons Attribution (CC BY) license (<https://creativecommons.org/licenses/by/4.0/>).

1. Introduction

Histone deacetylases (HDACs) are involved in a wide range of biological responses by histone deacetylation and nonhistone lysine post-translational modification and have been identified as targets in the treatment of various diseases, especially for cancer [1–5]. The HDACs family include class I (HDAC1, HDAC2, HDAC3, HDAC8), class II (HDAC4, HDAC5, HDAC6, HDAC7, HDAC9, HDAC10), class III (Sirt1–7), and class IV (HDAC11) [6]. To date, five HDACis have been approved to treat cutaneous T-cell lymphoma, peripheral T-cell lymphoma, or multiple myeloma [7–11]. However, all of them are nonselective or partially selective, which might have potentially toxic side effects [12,13]. In contrast with the lethal effect of HDAC1-3 genetic ablation, mice with HDAC6 knocked out are viable and develop normally [14,15]. HDAC6, mainly located in the cytoplasm, exhibits unique characteristics [16,17]. It contains two tandem catalytic domains and directly acts on a host of cytosolic proteins and substrates such as α - and β -tubulin, heat shock protein, assembled micro-tubules, and cortactin [18–20], which are closely related to tumorigenesis. Moreover, the binding to ubiquitin by the distinctive zinc finger domain makes HDAC6 regulate protein clearance and degradation [21]. The advantage of lower toxicity and improved safety profile has made the development of HDAC6i a hot research topic in cancer treatment [16,22–24].

To date, a lot of synthetic sHDAC6is have been reported [25–31]. The structure of HDAC6i typically contains three parts: (a) a zinc-binding group (ZBG) coordinating with Zn²⁺ ion at the bottom of the active site, (b) a linker region embedding in the hydrophobic tunnel between the catalytic site and the outer surface, and (c) a capping group overlaying on the surface (Figure 1). The clinical ACY-1215 (**1**) inhibited HDAC1 and HDAC6 with

IC₅₀s of 5 nM and 58 nM and was evaluated for the treatment of multiple myeloma (MM) and lymphoid malignancies [32]. ACY-1215 showed synergistic anti-MM activity together with bortezomib, resulting in protracted endoplasmic reticulum stress and apoptosis. ACY-241 (2), similar to the structure of ACY-1215, achieved higher serum concentrations than ACY-1215. The IC₅₀ value of ACY-241 against HDAC6 was 2.6 nM, 13–18-fold better than HDAC1–3 [33]. KA2507 (3) potently inhibited HDAC6 with IC₅₀ of 2.5 nM. It demonstrated antitumor efficacy and immune modulatory effects in preclinical models. In a phase I study, KA2507 showed selective target engagement, no significant toxicities, and prolonged disease stabilization in a subset of patients [34]. Despite great success in sHDAC6is discovery, available clinical agents are still rare, and the lack of therapeutic effect on solid tumors is another problem for HDAC inhibitors.

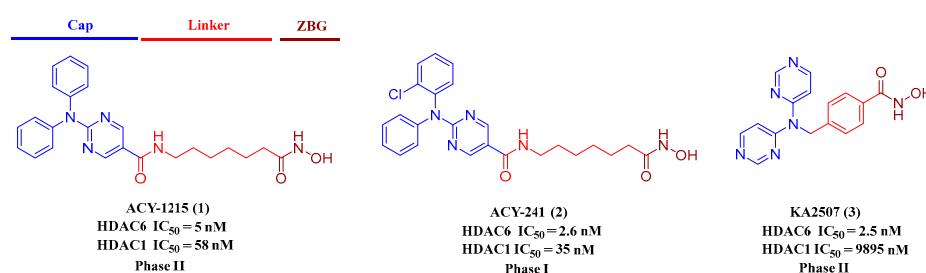


Figure 1. Representative selective HDAC6 inhibitors in clinic.

Because the cap region of the HDAC6 pocket is wider and larger than that of HDAC1 [35], a more rigid and bigger capping group might improve the selectivity toward HDAC6. For HDAC6is 1–3, the common feature is apparent: a “Y” shaped and predominantly aromatic capping group with hydroxamic acid as ZBG. The 5, 6, 7, 8-tetrahydropyrido[3, 4-*d*]pyrimidine (4) was frequently used in the development of kinase inhibitors for cancer treatment [36,37]. Hence, the introduction of such a scaffold in one molecule might be beneficial for the anticancer efficacy of HDAC6is. In this paper, we replaced the *N,N*-diphenylpyrimidine capping group of ACY1215 with 5, 6, 7, 8-tetrahydropyrido[3, 4-*d*]pyrimidine and retained the six-carbon linker as well as hydroxamic acid ZBG (Figure 2). Here, we reported the design, structure, and activity relationship (SAR) study and antiproliferative evaluation of these tetrahydropyridopyrimidines.

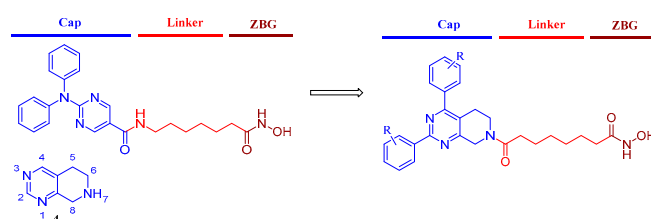
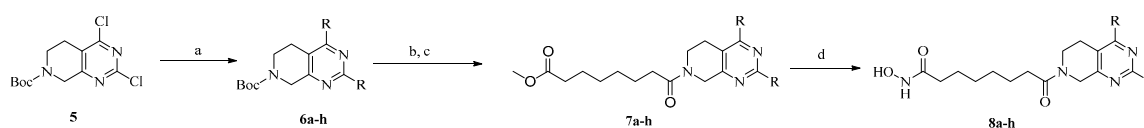


Figure 2. The design of tetrahydropyridopyrimidines as sHDAC6is.

2. Results and Discussion

2.1. Chemistry

The synthetic route to target compounds **8a–h** was initiated by the preparation of key intermediate **6a–h** from commercially available material **5** and two equivalent arylboronic acids by Suzuki reaction with Pd(dppf)Cl₂ as a catalyst and K₂CO₃ as a base (Scheme 1). For preliminary exploration, the same aryls were introduced on the C2 and C4 positions of the tetrahydropyridopyrimidine scaffold. Compounds **6a–h** underwent Boc deprotection under TFA/CH₂Cl₂ condition and subsequent condensation reaction with 8-methoxy-8-oxooctanoic acid through HATU, yielding the ester precursors **7a–h**. Then, **7a–h** was converted to the final hydroxamate product **8a–h** using aqueous hydroxylamine under basic conditions. Different electron-withdrawing or electron-donating substituents were introduced on two phenyls present in the capping part to explore the SAR. Moreover, the phenyl group was also replaced with an aromatic heterocycle such as thienyl or furyl.



Scheme 1. Reagents and conditions: (a) Pd(dppf)Cl₂, K₂CO₃, arylboronic acid, 1, 4-dioxane, 120 °C, 8 h; (b) TFA, dichloromethane (CH₂Cl₂), reflux, 2 h; (c) HATU, DIPEA, DMF, 0 °C, 6 h; (d) NH₂OH·HCl, KOH, 0 °C to r.t., 4 h.

2.2. HDAC1, 6 Activities and SAR Study of the Target Compounds

The target compounds **8a–h** were screened against HDAC6 with sHDAC6i ACY1215 and nonselective SAHA as the positive controls. Considering specific and redundant functions of class I HDACs in the control of proliferation as well as potential toxicity [38], HDAC1 was chosen for selectivity evaluation. As displayed in Table 1, all eight compounds demonstrated low nanomolar HDAC6 activity and two-digit selectivity against HDAC1. The most potent **8f**, with *meta*-OMe phenyls as the capping group, inhibited HDAC6 with an IC₅₀ value of 6.4 nM and showed 48-fold selectivity against HDAC1, better than that of ACY1215. In addition, unsubstituted **8a** also had an IC₅₀ of 16.2 nM and 35-fold selectivity. The introduction of *para*-OMe phenyl (**8c**) maintained the potency. Although -CF₃, -Me, or furyl were adopted, a slight decrease in HDAC6 inhibition was observed (**8b**, **8d**, and **8h**). For thienyl derivatives **8e** and **8g**, the position of the sulfur atom obviously affected the HDAC6 activity (25.7 nM vs. 54 nM, respectively). It seemed that the substituent on the phenyl cap was critical for enzymatic activity.

Table 1. Intro inhibitory activities of target compounds **8a–h** against HDAC1 and HDAC6 (IC₅₀, nM).

Compound	R	HDAC1	HDAC6	Selectivity Index
8a		565	16.2	35
8b		640	24.4	41
8c		472	9.6	49
8d		306	19.6	16
8e		423	25.7	16
8f		308	6.4	48
8g		891	54.0	17
8h		551	21.5	26
1	/	97.6	8.1	12
SAHA	/	4.3	7.4	0.6

IC₅₀ values for enzymatic inhibition of HDAC1 and HDAC6 enzyme. We ran experiments in duplicate, SD < 15%. Assays were performed by Reaction Biology Corporation (Malvern, PA, USA).

8f, with the highest potency, was chosen for a detailed screening against other HDACs, including class I HDACs (HDAC2, 3, 8), HDAC 4, 5 (class IIa), and HDAC6 (class IIb) with ACY1215, SAHA, and TMP269 (a selective class IIa inhibitor) [39] as references. As demonstrated in Table 2, **8f** shows highly selective inhibition (more than 48-fold over other subtypes) toward HDAC6, and its selectivity values were higher than those of reference compound ACY1215. The IC₅₀ values of **8f** against HDAC1-3 were 308 nM, 390 nM, and 411 nM, respectively. **8f** showed poor activity for HDAC4, 5 and 8. The results further validate the importance of tetrahydropyridopyrimidine with bulky capping groups to yield pronounced HDAC6 selective inhibition.

Table 2. The screen of **8f** against HDAC isozymes (IC₅₀, nM).

Compound	IC ₅₀						
	HDAC1	HDAC2	HDAC3	HDAC4	HDAC5	HDAC6	HDAC8
8f	308	390	411	>10,000	>10,000	6.4	510
SAHA	4.2	11.5	3.5	>10,000	8870	7.1	1033
1	62.5	47.5	50.0	7250	5100	5.1	150
TMP269	>10,000	>10,000	>10,000	0.133	0.090	ND	ND

IC₅₀ values for enzymatic inhibition of HDAC enzymes. We ran experiments in duplicate, SD < 15%. Assays were performed by Reaction Biology Corporation (Malvern, PA, USA). ND = not determined.

2.3. Western Blot Assay

To further determine the intracellular target specificity of **8f**, human MM cell line RPMI-8226 was treated at concentrations of 1, 5, and 10 μM, along with the reference HDAC6i ACY1215 and pan-inhibitor SAHA at 10 μM (Figure 3). **8f** was able to increase the levels of acetylated α-tubulin in a dose-dependent manner while inducing only modest changes in the levels of acetylated histone 3 (H3), similar to those found for the reference HDAC6i ACY-1215 at 10 μM. As expected, the pan-active HDACi SAHA increased levels of both acetylated α-tubulin and acetylated histone H3 significantly compared to the vehicle.

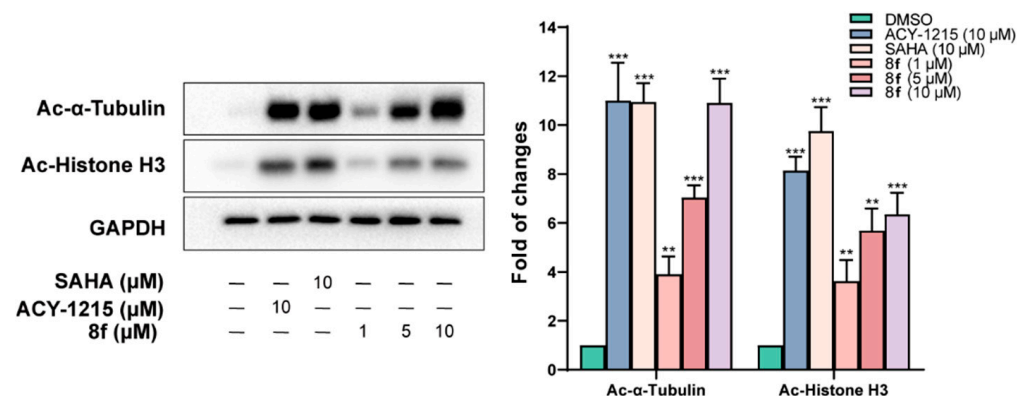


Figure 3. **8f** increases the levels of acetylated α-tubulin in a dose-dependent manner in RPMI-8226 cells—densitometric analyses of Ac-H3 and Ac-α-tubulin. Cells were treated for 24 h with compounds, and then Western blotting analysis was performed. ** $p < 0.01$, the *** $p < 0.001$ indicates comparison with the control group.

2.4. Molecular Simulation

The representative **8a** was docked into the human HDAC6 protein complex to elucidate the interaction model between these tetrahydropyridopyrimidines and the target protein. As outlined in Figure 4A, hydroxamate-Zn²⁺ coordination was modeled with bidentate geometry, and the Zn²⁺–O distances are 2.4 and 1.8 Å for the OH and C=O groups, respectively. The side chain of His610 additionally accepted a hydrogen bond from the hydroxamate OH group. The aliphatic chain linker embeds into the channel between Phe620 and Phe680. Moreover, two phenyl substituents of **8a** in the cap region were oriented

into the crevice formed by Met682, Asp567, and Ser564. Tetrahydropyridopyrimidine scaffold as a proper connecting unit made the capping group of **8a** match well with amino acids on the rim of the binding tunnel (Figure 4B). For compound **8f**, its polar *meta*-OMe group improved the HDAC6 activity. For comparison, ACY-1215 was also docked into the HDAC6 crystallographic structure, and the superimposition of ACY-1215 and **8a** was disclosed in Figure 4C. Both compounds occupied the same pocket and showed similar binding modes.

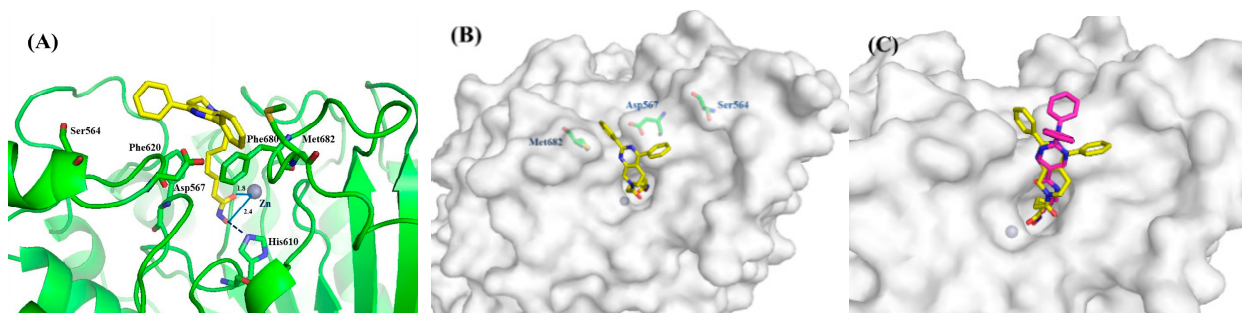


Figure 4. (A) Binding model of **8a** (yellow) in the catalytic pocket of human HDAC6 (PDB code: 5EDU). (B) Surface map of **8a** in the catalytic pocket of HDAC6 (grey). (C) The superimposition of ACY-1215 and **8a** in HDAC6. Key residues were labeled in green. The hydrogen bonds were labeled in blue. Zinc ion was shown in brown.

2.5. Antiproliferative Activities of Representative Compounds

Hematological tumors such as lymphoma, multiple myeloma, and chronic myeloid leukemia are more sensitive to HDAC inhibitors. Therefore, HL60 and RPMI-8226 tumor cells were used for antiproliferative biological tests of our compounds. Moreover, colon cancer cell HCT116 was also added to evaluate the antiproliferative effect for solid tumors of these tetrahydropyridopyrimidines. IC₅₀ values of three representative compounds **8a**, **8c**, and **8f** toward HL60 and RPMI-8226 cells range from 2.80 to 16.3 μ M, which indicated that these tetrahydropyridopyrimidines tested kept the cell-based activity (Table 3). For solid tumor cells HCT116, all three analogs exhibited promising efficacy, especially for **8c** and **8f**, with IC₅₀s of 4.72 and 3.25 μ M. This result rendered these new inhibitors valuable hits for applications beyond multiple myeloma.

Table 3. Antiproliferative effect of **8a**, **8c** and **8f** against HL60, HCT116 and RPMI-8226 cell lines (IC₅₀, μ M).

Compound	HL60	HCT116	RPMI-8226
8a	12.5	23.4	16.3
8c	3.78	4.72	4.63
8f	3.20	3.25	2.80
1	4.10	6.50	1.70
SAHA	0.87	4.50	0.66

IC₅₀ values are averages of three independent experiments, SD < 10%.

Then, **8f** was submitted to NCI for antiproliferative evaluation against 59 different tumor cell lines. The cancer types of the NCI-60 program include leukemia, non-small cell lung cancer (NSCLC), colon cancer, CNS cancer, melanoma, ovary cancer, renal cancer, prostate cancer, and breast cancer. As shown in Table 4, **8f** had an overall antiproliferative profile with percent inhibitions of 56 cell lines > 80% at 10 μ M concentration.

Table 4. Antiproliferative screening against 59 cell lines of **8f** (Inhibition% values at 10 μ M concentration).

Cancer Type	Cell Line	8f	Cancer Type	Cell Line	8f
Leukemia	CCRF-CEM	85.0	Ovarian Cancer	M14	90.5
	HL60	100		MDA-MB-435	95.8
	K-562	90.2		SK-MEL-2	100
	MOLT-4	87.7		SK-MEL-28	100
	RPMI-8226	88.7		SK-MEL-5	100
	SR	84.3		UACC-257	98.7
	A549/ATCC	87.7		UACC-62	100
	EKVX	84.4		IGROV1	100
	HOP-62	99.1		OVCAR-3	100
	HOP-92	100		OVCAR-4	67.1
Non-Small Cell Lung Cancer	NCI-H226	93.3	OVCAR-5	100	
	NCI-H23	100	OVCAR-8	93.6	
	NCI-H322M	89.0	NCI/ADR-RES	100	
	NCI-H460	95.5	SK-OV-3	100	
	NCI-H522	69.1	786-0	89.1	
	COLO 205	100	A498	100	
	HCC-2998	100	ACHN	100	
	HCT-116	96	CAKI-1	100	
	HCT-15	100	SN12C	100	
	HT29	95.3	TK-10	100	
Colon Cancer	KM12	88.4	UO-31	100	
	SW-620	100	PC-3	83.3	
	SF-268	92.2	DU-145	89.8	
	SF-295	100	MCF7	92.1	
	CNS Cancer	SF-539	99.0	MDA-MB-231/ATCC	100
		SNB-19	100	HS 578T	97.8
		SNB-75	71.0	BT-549	81.9
		U251	100	T-47D	100
	Melanoma	LOX IMVI	100	MDA-MB-468	100
		MALME-3M	100		

3. Experimental Section

3.1. Chemistry

All the starting reagents were purchased and were used with no additional purification. All the mentioned yields were for isolated products. Melting points were determined in open capillaries on a WRS-1A digital melting point apparatus (Shenguang). $^1\text{H-NMR}$ spectra were detected on a Bruker DRX-400 (400 MHz) using TMS as the internal standard. High-resolution mass spectra were obtained from Thermo Scientific Q Exactive. The chemical shifts were reported in ppm (δ), and coupling constants (J) values were given in Hertz (Hz). The purities of all target compounds were tested by HPLC to be >95.0%. HPLC analysis was performed at room temperature using an Agilent Eclipse XDB-C18 (250 mm \times 4.6 mm) and plotted at 254 nm by 30% MeOH/H₂O as a mobile phase.

3.1.1. Tert-Butyl 2, 4-Diphenyl-5, 8-dihydropyrido[3, 4-*d*]pyrimidine-7(6*H*)-carboxylate (**6a**)

To a stirred mixture of tert-butyl 2, 4-dichloro-5, 8-dihydropyrido[3, 4-*d*]pyrimidine-7(6*H*)-carboxylate (304.2 mg, 1 mmol), potassium carbonate (345.5 mg, 2.5 mmol) and Pd(dppf)Cl₂ (36.3 mg, 0.05 mmol) in 50 mL of 1, 4-dioxane was added phenylboronic acid (243.9 mg, 2 mmol). After stirring at reflux for 8 h under an argon atmosphere, the reaction mixture was concentrated under reduced pressure. Then, the reaction mixture was diluted with saturated sodium chloride (100 mL) and extracted with EtOAc (100 mL \times 3). The combined organic extracts were dried over anhydrous Na₂SO₄ and concentrated under reduced pressure. The white product was obtained by chromatography on a silica gel column with a yield of 96%. $^1\text{H-NMR}$ (400 MHz, DMSO-*d*₆) δ : 8.44–8.38 (m, 2H), 7.81–7.75 (m, 2H), 7.57–7.50 (m, 6H), 4.67 (s, 2H), 3.57 (s, 2H), 2.88 (t, J = 5.4 Hz, 2H), 1.47 (s, 9H).

3.1.2. Tert-Butyl 2, 4-di-p-tolyl-5, 8-dihydropyrido[3, 4-*d*]pyrimidine-7(6*H*)-carboxylate (**6b**)

6b was synthesized from (4-methylphenyl)boronic acid using a procedure similar to that described for the synthesis of **6a** and was obtained as a white solid (yield: 88%). ¹H-NMR (400 MHz, DMSO-*d*₆) δ: 8.32 (d, *J* = 8.9 Hz, 2H), 7.75 (d, *J* = 8.8 Hz, 2H), 7.07 (dd, *J* = 12.9, 8.9 Hz, 4H), 4.61 (s, 2H), 2.42 (s, 3H), 2.35 (s, 3H), 3.54 (s, 2H), 2.86 (t, *J* = 5.4 Hz, 2H), 1.47 (s, 9H).

3.1.3. Tert-Butyl 2, 4-Bis(4-methoxyphenyl)-5, 8-dihydropyrido[3, 4-*d*]pyrimidine-7(6*H*)-carboxylate (**6c**)

6c was synthesized from (4-methoxyphenyl)boronic acid using a procedure similar to that described for the synthesis of **6a** and was obtained as a white solid (yield: 90%). ¹H-NMR (400 MHz, DMSO-*d*₆) δ: 8.35 (d, *J* = 8.9 Hz, 2H), 7.77 (d, *J* = 8.8 Hz, 2H), 7.07 (dd, *J* = 12.9, 8.9 Hz, 4H), 4.62 (s, 2H), 3.84 (d, *J* = 6.1 Hz, 6H), 3.56 (s, 2H), 2.88 (t, *J* = 5.4 Hz, 2H), 1.47 (s, 9H).

3.1.4. Tert-Butyl 2, 4-Di(furan-3-yl)-5, 8-dihydropyrido[3, 4-*d*]pyrimidine-7(6*H*)-carboxylate (**6d**)

Similar to the synthesis of **6a**, **6d** was obtained from furan-3-ylboronic acid as a white solid (yield: 88%). ¹H-NMR (400 MHz, DMSO-*d*₆) δ: 8.43 (d, *J* = 12.1 Hz, 2H), 7.86 (s, 1H), 7.79 (s, 1H), 7.23 (s, 1H), 7.08 (s, 1H), 4.56 (s, 2H), 3.65 (s, 2H), 2.88 (t, *J* = 5.4 Hz, 2H), 1.45 (s, 9H).

3.1.5. Tert-Butyl 2, 4-Di(thiophen-3-yl)-5,8-dihydropyrido [3, 4-*d*]pyrimidine-7(6*H*)-carboxylate (**6e**)

Similar to the synthesis of **6a**, **6e** was obtained from thiophen-3-ylboronic acid as a white solid (yield: 87%). ¹H-NMR (400 MHz, DMSO-*d*₆) δ: 8.37 (d, *J* = 3.9 Hz, 1H), 8.24–8.20 (m, 1H), 7.83 (d, *J* = 6.0 Hz, 1H), 7.75 (d, *J* = 5.0 Hz, 1H), 7.71 (dd, *J* = 5.0, 2.8 Hz, 1H), 7.64 (dd, *J* = 5.0, 3.1 Hz, 1H), 4.60 (s, 2H), 3.61 (s, 2H), 2.97 (t, *J* = 5.4 Hz, 2H), 1.46 (s, 9H).

3.1.6. Tert-Butyl 2, 4-Bis(3-methoxyphenyl)-5, 8-dihydropyrido [3, 4-*d*]pyrimidine-7(6*H*)-carboxylate (**6f**)

Similar to the synthesis of **6a**, **6f** was obtained from (3-methoxyphenyl)boronic acid as a white solid (yield: 89%). ¹H-NMR (400 MHz, DMSO-*d*₆) δ: 8.00 (d, *J* = 7.8 Hz, 1H), 7.92 (s, 1H), 7.46–7.44 (m, 2H), 7.33–7.26 (m, 2H), 7.12–7.10 (m, 2H), 4.67 (s, 2H), 3.83 (s, 6H), 3.57 (s, 2H), 2.87 (t, *J* = 5.4 Hz, 2H), 1.47 (s, 9H).

3.1.7. Tert-Butyl 2, 4-Di(thiophen-2-yl)-5, 8-dihydropyrido [3, 4-*d*]pyrimidine-7(6*H*)-carboxylate (**6g**)

Similar to the synthesis of **6a**, **6g** was obtained from thiophen-2-ylboronic acid as a white solid (yield: 85%). ¹H-NMR (400 MHz, DMSO-*d*₆) δ: 7.94 (dd, *J* = 3.6, 1.1 Hz, 1H), 7.89 (d, *J* = 5.1 Hz, 1H), 7.85 (d, *J* = 3.7 Hz, 1H), 7.76 (dd, *J* = 5.0, 1.0 Hz, 1H), 7.30–7.27 (m, 1H), 7.23–7.20 (m, 1H), 4.59 (s, 2H), 3.67 (s, 2H), 3.04 (t, *J* = 5.5 Hz, 2H), 1.46 (s, 9H).

3.1.8. Tert-Butyl 2, 4-Bis(4-(trifluoromethyl)phenyl)-5, 8-dihydropyrido [3, 4-*d*]pyrimidine-7(6*H*)-carboxylate (**6h**)

Similar to the synthesis of **6a**, **6h** was obtained from (4-(trifluoromethyl)phenyl)boronic acid as a white solid (yield: 92%). ¹H-NMR (400 MHz, DMSO-*d*₆) δ: 8.60 (d, *J* = 8.2 Hz, 2H), 8.01 (d, *J* = 8.2 Hz, 2H), 7.95–7.84 (m, 4H), 4.72 (s, 2H), 3.59 (s, 2H), 2.90 (t, *J* = 5.4 Hz, 2H), 1.47 (s, 9H).

3.1.9. Methyl 8-(2, 4-Diphenyl-5, 8-dihydropyrido [3, 4-*d*]pyrimidin-7(6*H*)-yl)-8-oxooctanoate (**7a**)

(i) To a stirred mixture of **6a** (387.5 mg, 1 mmol) in CH₂Cl₂ (40 mL) was added TFA (5 mL) in portions. The reaction mixture was stirred at reflux for 2 h and then concentrated under reduced pressure. The reaction mixture was diluted with saturated sodium chloride (50 mL) and adjusted to PH = 7 with Na₂CO₃ saturated solution. Then, the mixture

was extracted with EtOAc (50 mL \times 3). The combined organic extracts were dried over anhydrous Na₂SO₄ and concentrated under reduced pressure. The product was obtained as an oil. (ii) To a solution of the product acquired in step (i) in DMF (30 mL) was added HATU (1 mmol) DIPEA (4 mmol) at 0 °C. Then, the reaction mixture was stirred at room temperature overnight. After the completion of the reaction detected by TLC, the reaction was poured into water (30 mL) and extracted with EtOAc (60 mL \times 3). The combined organic extracts were dried over anhydrous Na₂SO₄ and concentrated under reduced pressure. Then, the resulting mixture was purified by column chromatography to give the product **7a** with 54% isolated yield: white solid. ¹H-NMR (400 MHz, DMSO-*d*₆) δ : 8.41 (s, 2H), 7.77 (d, *J* = 3.5 Hz, 2H), 7.59–7.46 (m, 6H), 4.79 (d, *J* = 21.8 Hz, 2H), 3.67 (t, *J* = 5.1 Hz, 2H), 3.57 (s, 3H), 2.93 (t, *J* = 5.2 Hz, 1H), 2.82 (t, *J* = 5.2 Hz, 1H), 2.49–2.37 (m, 2H), 2.32–2.22 (m, 2H), 1.53 (m, 4H), 1.30 (d, *J* = 3.6 Hz, 4H).

3.1.10. Methyl 8-(2, 4-di-p-tolyl-5, 8-dihydropyrido [3, 4-*d*]pyrimidin-7(6*H*)-yl)-8-oxooctanoate (**7b**)

Similar to the synthesis of **7a**, **7b** was obtained as a white solid with a yield of 49%. ¹H-NMR (400 MHz, DMSO-*d*₆) δ : 8.31 (dd, *J* = 8.2, 2.0 Hz, 2H), 7.68 (dd, *J* = 8.1, 2.4 Hz, 2H), 7.34 (dd, *J* = 14.1, 8.1 Hz, 4H), 4.78 (d, *J* = 28.1 Hz, 2H), 3.68 (t, *J* = 5.4 Hz, 2H), 3.57 (s, 3H), 2.94 (t, *J* = 5.2 Hz, 1H), 2.83 (t, *J* = 5.2 Hz, 1H), 2.48–2.42 (m, 2H), 2.40 (s, 3H), 2.38 (s, 3H), 2.31–2.28 (m, 2H), 1.58–1.47 (m, 4H), 1.35–1.22 (m, 4H).

3.1.11. Methyl 8-(2, 4-Bis(4-methoxyphenyl)-5, 8-dihydropyrido [3, 4-*d*]pyrimidin-7(6*H*)-yl)-8-oxooctanoate (**7c**)

Similar to the synthesis of **7a**, **7c** was obtained as a yellow solid with a yield of 38%. ¹H-NMR (400 MHz, DMSO-*d*₆) δ : 8.35 (d, *J* = 8.5 Hz, 2H), 7.76 (d, *J* = 8.0 Hz, 2H), 7.07 (dd, *J* = 12.9, 8.5 Hz, 4H), 4.74 (d, *J* = 26.0 Hz, 2H), 3.83 (m, 6H), 3.67 (s, 2H), 3.57 (s, 3H), 2.94 (s, 1H), 2.83 (s, 1H), 2.43 (dd, *J* = 12.2, 6.4 Hz, 2H), 2.29 (t, *J* = 5.7 Hz, 2H), 1.53–1.51 (m, 4H), 1.34–1.25 (m, 4H).

3.1.12. Methyl 8-(2, 4-Di(furan-3-yl)-5, 8-dihydropyrido [3, 4-*d*]pyrimidin-7(6*H*)-yl)-8-oxooctanoate (**7d**)

Similar to the synthesis of **7a**, **7d** was obtained as a yellow solid with a yield of 43%. ¹H-NMR (400 MHz, DMSO-*d*₆) δ : 8.44 (s, 1H), 8.23–8.10 (m, 2H), 7.85 (s, 1H), 7.67 (d, *J* = 4.2 Hz, 1H), 7.20 (d, *J* = 3.0 Hz, 1H), 7.05 (s, 1H), 4.66 (d, *J* = 16.7 Hz, 2H), 3.77 (s, 2H), 3.56 (s, 3H), 2.94 (s, 1H), 2.83 (s, 1H), 2.42 (m, 2H), 1.91 (q, *J* = 6.9 Hz, 2H), 1.45 (dd, *J* = 16.1, 9.0 Hz, 4H), 1.38–1.15 (m, 4H).

3.1.13. Methyl 8-(2, 4-Di(thiophen-3-yl)-5, 8-dihydropyrido [3, 4-*d*]pyrimidin-7(6*H*)-yl)-8-oxooctanoate (**7e**)

Similar to the synthesis of **7a**, **7e** was obtained as a white solid with a yield of 41%. ¹H-NMR (400 MHz, DMSO-*d*₆) δ : 8.38 (dd, *J* = 3.0, 1.1 Hz, 1H), 8.23–8.18 (m, 1H), 7.84 (d, *J* = 5.0 Hz, 1H), 7.78–7.69 (m, 2H), 7.66–7.62 (m, 1H), 4.73 (d, *J* = 21.2 Hz, 2H), 3.73 (t, *J* = 4.3 Hz, 2H), 3.57 (d, *J* = 2.7 Hz, 3H), 3.04 (t, *J* = 5.3 Hz, 1H), 2.94 (t, *J* = 5.2 Hz, 1H), 2.44 (t, *J* = 7.4 Hz, 2H), 2.28 (q, *J* = 7.1 Hz, 2H), 1.52–1.50 (m, 4H), 1.34–1.24 (m, 4H).

3.1.14. Methyl 8-(2, 4-Bis(3-methoxyphenyl)-5, 8-dihydropyrido [3, 4-*d*]pyrimidin-7(6*H*)-yl)-8-oxooctanoate (**7f**)

Similar to the synthesis of **7a**, **7f** was obtained as a yellow solid with a yield of 48%. ¹H-NMR (400 MHz, DMSO-*d*₆) δ : 8.46 (s, 1H), 7.98 (d, *J* = 7.8 Hz, 1H), 7.90 (s, 1H), 7.47–7.40 (m, 2H), 7.32–7.21 (m, 2H), 7.04 (m, 2H), 4.80 (d, *J* = 26.2 Hz, 2H), 3.82 (s, 6H), 3.65 (t, *J* = 5.5 Hz, 2H), 3.57 (s, 3H), 2.92 (t, *J* = 5.1 Hz, 1H), 2.82 (t, *J* = 5.1 Hz, 1H), 2.45–2.35 (m, 2H), 1.92 (t, *J* = 7.3 Hz, 2H), 1.50–1.48 (m, 4H), 1.26 (q, *J* = 16.1, 12.5 Hz, 4H).

3.1.15. Methyl 8-(2, 4-Di(thiophen-2-yl)-5, 8-dihydropyrido [3, 4-*d*]pyrimidin-7(6*H*)-yl)-8-oxooctanoate (**7g**)

Similar to the synthesis of **7a**, **7g** was obtained as a yellow solid with a yield of 49%. ¹H-NMR (400 MHz, DMSO-*d*₆) δ: 8.36 (s, 1H), 7.90 (d, *J* = 4.5 Hz, 1H), 7.65 (d, *J* = 5.0 Hz, 1H), 7.77 (t, *J* = 4.3 Hz, 1H), 7.70 (d, *J* = 4.8 Hz, 1H), 7.26 (q, *J* = 5.0 Hz, 1H), 7.23–7.17 (m, 1H), 4.71 (d, *J* = 23.0 Hz, 2H), 3.83–3.70 (m, 2H), 3.57 (s, 3H), 3.11 (t, *J* = 5.1 Hz, 1H), 2.96 (t, *J* = 5.2 Hz, 1H), 2.47–2.42 (m, 2H), 1.93–1.91 (m, 2H), 1.56–1.41 (m, 4H), 1.33–1.16 (m, 4H).

3.1.16. Methyl 8-(2, 4-Bis(4-(trifluoromethyl)phenyl)-5, 8-dihydropyrido [3, 4-*d*]pyrimidin-7(6*H*)-yl)-8-oxooctanoate (**7h**)

Similar to the synthesis of **7a**, **7g** was obtained as a yellow solid with a yield of 46%. ¹H-NMR (400 MHz, DMSO-*d*₆) δ: 8.34 (s, 1H), 8.19 (d, *J* = 8.2 Hz, 2H), 8.00 (d, *J* = 8.1 Hz, 2H), 7.90 (dd, *J* = 12.7, 8.3 Hz, 4H), 4.82 (d, *J* = 27.8 Hz, 2H), 3.71–3.60 (m, 2H), 2.92 (t, *J* = 4.8 Hz, 1H), 2.81 (t, *J* = 4.7 Hz, 1H), 2.42–2.33 (m, 2H), 1.93 (t, *J* = 7.3 Hz, 2H), 1.51–1.49 (m, 4H), 1.36–1.15 (m, 4H).

3.1.17. 8-(2, 4-Diphenyl-5, 8-dihydropyrido [3, 4-*d*]pyrimidin-7(6*H*)-yl)-*N*-hydroxy-8-oxooctanamide (**8a**)

A solution of NH₂OH·HCl (1.70 g, 24.46 mmol) in MeOH (9 mL) was combined with KOH (1.70 g, 30.29 mmol) at 0 °C in an ice bath. Then, the mixture was stirred for 30 min and filtered. **7a** (457.6 mg, 1 mmol) was added to the filtrate, and the reaction was stirred for an additional 4 h at 0 °C in an ice bath. The resulting mixture was poured into water (30 mL), and the pH value was adjusted to 7. The mixture was diluted with saturated NaCl aqueous solution (40 mL) and extracted with EtOAc (50 mL × 3). After drying over Na₂SO₄, the organic phase was concentrated and purified by column chromatography to give the product **8a**. 84% yield; white solid; m.p.: 115–117 °C. ¹H-NMR (400 MHz, DMSO-*d*₆) δ: 10.35 (s, 1H), 8.67 (s, 1H), 8.45–8.39 (m, 2H), 7.80–7.74 (m, 2H), 7.56–7.52 (m, 6H), 4.80 (d, *J* = 24.4 Hz, 2H), 3.69 (t, *J* = 5.5 Hz, 2H), 2.95 (t, *J* = 5.1 Hz, 1H), 2.84 (t, *J* = 5.1 Hz, 1H), 2.48–2.40 (m, 2H), 1.95 (t, *J* = 7.3 Hz, 2H), 1.53–1.51 (m, 4H), 1.34–1.22 (m, 4H). ¹³C-NMR (101 MHz, DMSO-*d*₆) δ: 171.24, 169.14, 164.54, 163.38, 160.67, 137.33, 137.03, 130.63, 129.61, 129.07, 128.64, 128.36, 127.62, 123.75, 46.44, 42.13, 32.66, 32.26, 28.49, 26.70, 25.88, 25.06, 24.54. HR-MS (ESI, *m/z*): Calcd for 459.23907 (C₂₇H₃₁N₄O₃⁺ [M + H]⁺). Found 459.23901.

3.1.18. 8-(2, 4-di-*p*-tolyl-5, 8-dihydropyrido [3, 4-*d*]pyrimidin-7(6*H*)-yl)-*N*-hydroxy-8-oxooctanamide (**8b**)

Similar to the synthesis of **8a**, **8b** was obtained from **7b** as a white solid (yield: 64%). M.p.: 110–112 °C. ¹H-NMR (400 MHz, DMSO-*d*₆) δ: 10.35 (s, 1H), 8.68 (s, 1H), 8.31 (dd, *J* = 8.2, 2.2 Hz, 2H), 7.69 (dd, *J* = 8.1, 2.7 Hz, 2H), 7.37 (s, 1H), 7.36–7.33 (m, 2H), 7.32 (d, *J* = 1.9 Hz, 1H), 4.78 (d, *J* = 28.7 Hz, 2H), 3.68 (t, *J* = 4.9 Hz, 2H), 2.95 (t, *J* = 5.2 Hz, 1H), 2.84 (t, *J* = 5.3 Hz, 1H), 2.45 (d, *J* = 7.1 Hz, 2H), 2.41 (s, 3H), 2.38 (s, 3H), 1.94 (t, *J* = 7.3 Hz, 2H), 1.51 (m, 4H), 1.33–1.24 (m, 4H). ¹³C-NMR (101 MHz, DMSO-*d*₆) δ: 171.21, 169.16, 164.34, 163.14, 160.68, 140.35, 139.36, 139.32, 134.57, 134.44, 129.23, 129.07, 128.90, 127.59, 123.35, 123.22, 46.45, 42.19, 32.27, 28.50, 26.78, 25.08, 24.55, 24.44, 20.96. HR-MS (ESI, *m/z*): Calcd for 487.27037 (C₂₉H₃₅N₄O₃⁺ [M + H]⁺). Found 487.27020.

3.1.19. 8-(2, 4-Bis(4-methoxyphenyl)-5, 8-dihydropyrido [3, 4-*d*]pyrimidin-7(6*H*)-yl)-*N*-hydroxy-8-oxooctanamide (**8c**)

Similar to the synthesis of **8a**, **8c** was obtained from **7c** as a white solid (yield: 57%). M.p.: 117–118 °C. ¹H-NMR (400 MHz, DMSO-*d*₆) δ: 10.35 (s, 1H), 8.68 (s, 1H), 8.38 (d, *J* = 2.0 Hz, 1H), 8.35 (d, *J* = 2.0 Hz, 1H), 7.77 (d, *J* = 8.6 Hz, 2H), 7.12–7.10 (m, 1H), 7.09–7.06 (m, 2H), 7.05 (d, *J* = 2.6 Hz, 1H), 4.76 (d, *J* = 28.2 Hz, 2H), 3.85 (s, 3H), 3.83 (s, 3H), 3.68 (t, *J* = 5.3 Hz, 2H), 2.96 (t, *J* = 4.9 Hz, 1H), 2.85 (t, *J* = 5.1 Hz, 1H), 2.45 (dd, *J* = 13.6, 6.6 Hz, 2H), 1.94 (t, *J* = 7.3 Hz, 2H), 1.51 (m, 4H), 1.34–1.21 (m, 4H). ¹³C-NMR (101 MHz, DMSO-*d*₆) δ: 169.12, 161.96, 161.34, 160.43, 144.74, 138.38, 137.87, 130.83, 130.78, 129.69, 129.65, 129.23,

120.97, 120.82, 113.96, 113.73, 46.46, 46.07, 32.25, 28.49, 28.46, 26.87, 25.05, 24.54, 24.42. HR-MS (ESI, m/z): Calcd for 519.26020 ($C_{29}H_{35}N_4O_5^+$ [$M + H$] $^+$). Found 519.26001.

3.1.20. 8-(2, 4-Di(furan-3-yl)-5, 8-dihydropyrido [3, 4-*d*]pyrimidin-7(6*H*)-yl)-*N*-hydroxy-8-oxooctanamide (**8d**)

Similar to the synthesis of **8a**, **8d** was obtained from **7d** as a white solid (yield: 65%). M.p.: 104~106 °C. 1H -NMR (400 MHz, DMSO- d_6) δ : 10.35 (s, 1H), 8.70 (s, 1H), 8.46–8.35 (m, 2H), 7.87 (s, 1H), 7.80 (d, $J = 4.2$ Hz, 1H), 7.23 (d, $J = 3.0$ Hz, 1H), 7.08 (s, 1H), 4.69 (d, $J = 16.7$ Hz, 2H), 3.77 (s, 2H), 2.96 (s, 1H), 2.85 (s, 1H), 2.43 (q, $J = 7.0$ Hz, 2H), 1.95–1.93 (m, 2H), 1.50 (dd, $J = 16.1, 9.0$ Hz, 4H), 1.39–1.17 (m, 4H). ^{13}C -NMR (101 MHz, DMSO- d_6) δ : 171.16, 171.09, 169.20, 166.19, 162.91, 145.19, 144.70, 144.46, 143.81, 126.54, 124.08, 122.12, 121.94, 46.25, 41.98, 32.58, 32.28, 32.05, 28.48, 26.38, 25.07, 24.57. HR-MS (ESI, m/z): Calcd for 439.19760 ($C_{29}H_{35}N_4O_5^+$ [$M + H$] $^+$). Found 439.19751.

3.1.21. 8-(2, 4-Di(thiophen-3-yl)-5,8-dihydropyrido [3, 4-*d*]pyrimidin-7(6*H*)-yl)-*N*-hydroxy-8-oxooctanamide (**8e**)

Similar to the synthesis of **8a**, **8e** was obtained from **7e** as a white solid (yield: 68%). M.p.: 123~124 °C. 1H -NMR (400 MHz, DMSO- d_6) δ : 10.35 (s, 1H), 8.68 (s, 1H), 8.40–8.36 (m, 1H), 8.22 (d, $J = 8.8$ Hz, 1H), 7.84 (d, $J = 5.0$ Hz, 1H), 7.78–7.69 (m, 2H), 7.65 (m, 1H), 4.74 (d, $J = 21.9$ Hz, 2H), 3.73 (t, $J = 5.4$ Hz, 2H), 3.05 (t, $J = 5.0$ Hz, 1H), 2.94 (t, $J = 5.0$ Hz, 1H), 2.45 (t, $J = 7.2$ Hz, 2H), 2.00–1.87 (m, 2H), 1.61–1.40 (m, 4H), 1.36–1.21 (m, 4H). ^{13}C -NMR (101 MHz, DMSO- d_6) δ : 171.18, 171.09, 169.16, 163.39, 163.09, 141.12, 138.75, 129.23, 129.00, 128.77, 127.87, 127.17, 127.01, 126.35, 46.42, 42.14, 38.03, 32.27, 32.11, 26.79, 26.02, 25.06, 24.55. HR-MS (ESI, m/z): Calcd for 471.15191 ($C_{23}H_{27}N_4O_3S_2^+$ [$M + H$] $^+$). Found 471.15195.

3.1.22. 8-(2, 4-Bis(3-methoxyphenyl)-5, 8-dihydropyrido [3, 4-*d*]pyrimidin-7(6*H*)-yl)-*N*-hydroxy-8-oxooctanamide (**8f**)

Similar to the synthesis of **8a**, **8f** was obtained from **7f** as a white solid (yield: 64%). M.p.: 117~118 °C. 1H -NMR (400 MHz, DMSO- d_6) δ : 10.34 (s, 1H), 8.67 (s, 1H), 8.00 (d, $J = 7.8$ Hz, 1H), 7.93 (s, 1H), 7.50–7.40 (m, 2H), 7.33–7.25 (m, 2H), 7.10 (td, $J = 8.1, 2.2$ Hz, 2H), 4.80 (d, $J = 26.2$ Hz, 2H), 3.83 (s, 6H), 3.69 (t, $J = 5.5$ Hz, 2H), 2.94 (t, $J = 5.1$ Hz, 1H), 2.83 (t, $J = 5.1$ Hz, 1H), 2.48–2.39 (m, 2H), 1.94 (t, $J = 7.3$ Hz, 2H), 1.52–1.50 (m, 4H), 1.27–1.25 (m, 4H). ^{13}C -NMR (101 MHz, DMSO- d_6) δ : 171.25, 169.14, 164.41, 163.35, 160.40, 159.57, 159.15, 138.68, 138.50, 129.78, 129.55, 123.96, 121.26, 120.09, 116.35, 115.34, 115.13, 114.54, 114.39, 112.67, 46.44, 42.10, 32.26, 32.14, 28.49, 26.68, 25.88, 25.07, 24.54. HR-MS (ESI, m/z): Calcd for 519.26020 ($C_{29}H_{35}N_4O_5^+$ [$M + H$] $^+$). Found 519.26019.

3.1.23. 8-(2, 4-Di(thiophen-2-yl)-5, 8-dihydropyrido [3, 4-*d*]pyrimidin-7(6*H*)-yl)-*N*-hydroxy-8-oxooctanamide (**8g**)

Similar to the synthesis of **8a**, **8g** was obtained from **7g** as a white solid (yield: 71%). M.p.: 128~129 °C. 1H -NMR (400 MHz, DMSO- d_6) δ : 10.34 (s, 1H), 8.66 (s, 1H), 7.94 (d, $J = 4.5$ Hz, 1H), 7.90 (d, $J = 5.0$ Hz, 1H), 7.83 (t, $J = 4.3$ Hz, 1H), 7.76 (d, $J = 4.8$ Hz, 1H), 7.29 (q, $J = 5.0$ Hz, 1H), 7.24–7.19 (m, 1H), 4.73 (d, $J = 23.0$ Hz, 2H), 3.86–3.72 (m, 2H), 3.12 (t, $J = 5.1$ Hz, 1H), 2.99 (t, $J = 5.2$ Hz, 1H), 2.48–2.43 (m, 2H), 1.95–1.93 (m, 2H), 1.57–1.43 (m, 4H), 1.34–1.20 (m, 4H). ^{13}C -NMR (101 MHz, DMSO- d_6) δ : 171.15, 169.12, 163.90, 163.60, 157.29, 142.32, 141.57, 131.36, 131.12, 130.96, 130.56, 128.86, 128.59, 128.50, 49.31, 46.34, 32.25, 32.02, 28.45, 26.84, 26.03, 25.05, 24.54. HR-MS (ESI, m/z): Calcd for 471.15191 ($C_{23}H_{27}N_4O_3S_2^+$ [$M + H$] $^+$). Found 471.15192.

3.1.24. 8-(2, 4-Bis(4-(trifluoromethyl)phenyl)-5, 8-dihydropyrido [3, 4-*d*]pyrimidin-7(6*H*)-yl)-*N*-hydroxy-8-oxooctanamide (**8h**)

Similar to the synthesis of **8a**, **8h** was obtained from **7h** as a white solid (yield: 64%). M.p.: 145~146 °C. 1H -NMR (400 MHz, DMSO- d_6) δ : 10.33 (s, 1H), 8.65 (s, 1H), 8.61 (d, $J = 8.2$ Hz, 2H), 8.02 (d, $J = 8.1$ Hz, 2H), 7.92 (dd, $J = 12.7, 8.3$ Hz, 4H), 4.87 (d, $J = 27.8$ Hz, 2H), 3.77–3.66 (m, 2H), 2.97 (t, $J = 4.8$ Hz, 1H), 2.87 (t, $J = 4.7$ Hz, 1H), 2.48–2.38 (m, 2H),

1.94 (t, $J = 7.3$ Hz, 2H), 1.52 (m, 4H), 1.37–1.17 (m, 4H). ^{13}C -NMR (101 MHz, $\text{DMSO-}d_6$) δ : 169.12, 164.17, 163.60, 163.52, 159.39, 142.42, 130.07, 130.05, 130.02, 129.98, 128.36, 125.73, 125.69, 125.37, 125.34, 46.39, 41.93, 32.24, 32.22, 32.09, 28.48, 28.44, 25.04, 24.50. HR-MS (ESI, m/z): Calcd for 595.21384 ($\text{C}_{29}\text{H}_{29}\text{F}_6\text{N}_4\text{O}_3^+[\text{M} + \text{H}]^+$). Found 595.21344.

3.2. In Vitro HDAC Enzyme Assay

IC_{50} testing of compounds was performed by the Reaction Biology Corporation. The procedure was conducted as described previously [40].

3.3. Cell Culture and Antiproliferative Assay

The cells were cultured in IMDM (Gibco) medium with 20% FBS (Lonsera), 100 U/mL penicillin, and 100 $\mu\text{g}/\text{mL}$ streptomycin (Solarbio). All cells were maintained at 37 °C in a humidified atmosphere of 5% CO_2 in air. Briefly, 100 μL cell suspension or completed medium was plated into a 96-well plate. Compounds were added and incubated for 72 h. Then, 22 μL Alamar blue solution (1 mM) was pipetted into each well of a 96-well plate, and the plate was incubated for an additional 5~6 h. The absorbance (OD) was read at 530/590 nm. Data were normalized to vehicle groups (DMSO) and represented as the means of three independent measurements with standard errors of <20%. The IC_{50} values were calculated using Prism 5.0.

3.4. Western Blotting Assay

RPMI-8226 cells (1×10^6) were seeded overnight and incubated with compound **8f** for 24 h on indicated concentrations. Cell extract was prepared by lysing cultured cells with a mammalian protein extraction reagent supplemented with EDTA-free protease inhibitor for 15 min. SDS-PAGE and immunoblot analysis were conducted as described [40]. Antibodies for Ac-H3 (abcom, AB32129) and Ac- α -tubulin (Cell Signaling, 2144) were used.

3.5. Computational Methods

Molecular simulation was performed in Discovery Studio 3.0 software (BIOVIA, 5005 Wateridge Vista Drive, San Diego, CA, USA). Docking was conducted using cdocker based on the cocrystal of HDAC6 (PDB: 5EDU). The cavity occupied by trichostatin A was selected as the ligand binding site. The parameter setting was performed as previously reported [2].

4. Conclusions

In this work, a series of novel hybrid HDAC6 inhibitors were designed by chemically merging the structure of tetrahydropyridopyrimidine into the pharmacophore of HDAC6is. All newly synthesized compounds were first evaluated for inhibition of HDAC1 and HDAC6. All these diarylpyrimidine derivatives demonstrated potent HDAC6 activity at a nanomolar level and 16~49-fold selectivity over HDAC1. Western blot study further confirmed HDAC6 selectivity of these tetrahydropyridopyrimidines. In the cytotoxic assay, compounds **8a**, **8c**, and **8f** showed potent antiproliferative activity against representative hematological and solid tumors. Taken together, this work highlights the application of tetrahydropyridopyrimidine scaffold in the development of novel sHDAC6 inhibitors. These tetrahydropyridopyrimidine derivatives might be developed as new antitumor agents besides multiple myeloma. Further structural modification was performed in our lab.

Supplementary Materials: The following supporting information can be downloaded at: <https://www.mdpi.com/article/10.3390/molecules28217323/s1>. ^1H -NMR, ^{13}C -NMR and HR-MS spectras of synthesized compounds (1–8); Growth percents of **8f** against 59 tumor cells in NCI-60 program (9).

Author Contributions: Conception and Design: B.W., Y.L. and X.C.; Collection and Assembly of Data: B.W., Y.L. and L.Z.; Data Analysis and Interpretation: Y.W. and Z.L.; Administrative Support: B.W. and Y.L.; Manuscript Writing: B.W., Y.L. and X.C. All authors have read and agreed to the published version of the manuscript.

Funding: This work was supported by the key scientific research project of colleges and universities in Henan Province (23B320011).

Institutional Review Board Statement: Not applicable.

Informed Consent Statement: Not applicable.

Data Availability Statement: Data are contained within the article and Supplementary Material.

Conflicts of Interest: The authors declare no conflict of interest.

Sample Availability: Samples of the target compounds are available from the authors.

References

1. Minucci, S.; Pelicci, P.G. Histone deacetylase inhibitors and the promise of epigenetic (and more) treatments for cancer. *Nat. Rev. Cancer* **2006**, *6*, 38–51. [[CrossRef](#)]
2. Liang, T.; Xie, Z.; Dang, B.; Wang, J.; Zhang, T.; Luan, X.; Lu, T.; Cao, C.; Chen, X. Discovery of indole-piperazine derivatives as selective histone deacetylase 6 inhibitors with neurite outgrowth-promoting activities and neuroprotective activities. *Bioorg. Med. Chem. Lett.* **2023**, *81*, 129148. [[CrossRef](#)] [[PubMed](#)]
3. Falkenberg, K.J.; Johnstone, R.W. Histone deacetylases and their inhibitors in cancer, neurological diseases and immune disorders. *Nat. Rev. Drug Discov.* **2014**, *13*, 673–691. [[CrossRef](#)] [[PubMed](#)]
4. Bolden, J.E.; Peart, M.J.; Johnstone, R.W. Anticancer activities of histone deacetylase inhibitors. *Nat. Rev. Drug Discov.* **2006**, *5*, 769–784. [[CrossRef](#)] [[PubMed](#)]
5. Dasko, M.; de Pascual-Teresa, B.; Ortin, I.; Ramos, A. HDAC Inhibitors: Innovative Strategies for Their Design and Applications. *Molecules* **2022**, *27*, 715. [[CrossRef](#)] [[PubMed](#)]
6. Gregoret, I.V.; Lee, Y.M.; Goodson, H.V. Molecular evolution of the histone deacetylase family: Functional implications of phylogenetic analysis. *J. Mol. Biol.* **2004**, *338*, 17–31. [[CrossRef](#)] [[PubMed](#)]
7. Ning, Z.Q.; Li, Z.B.; Newman, M.J.; Shan, S.; Wang, X.H.; Pan, D.S.; Zhang, J.; Dong, M.; Du, X.; Lu, X.P. Chidamide (CS055/HBI-8000): A new histone deacetylase inhibitor of the benzamide class with antitumor activity and the ability to enhance immune cell-mediated tumor cell cytotoxicity. *Cancer Chemother. Pharmacol.* **2012**, *69*, 901–909. [[CrossRef](#)] [[PubMed](#)]
8. Laubach, J.P.; Moreau, P.; San-Miguel, J.F.; Richardson, P.G. Panobinostat for the Treatment of Multiple Myeloma. *Clin. Cancer Res.* **2015**, *21*, 4767–4773. [[CrossRef](#)] [[PubMed](#)]
9. Marks, P.A.; Breslow, R. Dimethyl sulfoxide to vorinostat: Development of this histone deacetylase inhibitor as an anticancer drug. *Nat. Biotechnol.* **2007**, *25*, 84–90. [[CrossRef](#)]
10. Sawas, A.; Radeski, D.; O'Connor, O.A. Belinostat in patients with refractory or relapsed peripheral T-cell lymphoma: A perspective review. *Ther. Adv. Hematol.* **2015**, *6*, 202–208. [[CrossRef](#)]
11. VanderMolen, K.M.; McCulloch, W.; Pearce, C.J.; Oberlies, N.H. Romidepsin (Istodax, NSC 630176, FR901228, FK228, depsipeptide): A natural product recently approved for cutaneous T-cell lymphoma. *J. Antibiot.* **2011**, *64*, 525–531. [[CrossRef](#)] [[PubMed](#)]
12. Dallavalle, S.; Pisano, C.; Zunino, F. Development and therapeutic impact of HDAC6-selective inhibitors. *Biochem. Pharmacol.* **2012**, *84*, 756–765. [[CrossRef](#)] [[PubMed](#)]
13. Benedetti, R.; Conte, M.; Altucci, L. Targeting Histone Deacetylases in Diseases: Where Are We? *Antioxid. Redox Signal.* **2015**, *23*, 99–126. [[CrossRef](#)] [[PubMed](#)]
14. Govindarajan, N.; Rao, P.; Burkhardt, S.; Sananbenesi, F.; Schluter, O.M.; Bradke, F.; Lu, J.; Fischer, A. Reducing HDAC6 ameliorates cognitive deficits in a mouse model for Alzheimer's disease. *EMBO Mol. Med.* **2013**, *5*, 52–63. [[CrossRef](#)]
15. Witt, O.; Deubzer, H.E.; Milde, T.; Oehme, I. HDAC family: What are the cancer relevant targets? *Cancer Lett.* **2009**, *277*, 8–21. [[CrossRef](#)]
16. Kalin, J.H.; Bergman, J.A. Development and therapeutic implications of selective histone deacetylase 6 inhibitors. *J. Med. Chem.* **2013**, *56*, 6297–6313. [[CrossRef](#)] [[PubMed](#)]
17. LoPresti, P. HDAC6 in Diseases of Cognition and of Neurons. *Cells* **2020**, *10*, 12. [[CrossRef](#)]
18. Rao, R.; Fiskus, W.; Ganguly, S.; Kambhampati, S.; Bhalla, K.N. HDAC inhibitors and chaperone function. *Adv. Cancer Res.* **2012**, *116*, 239–262.
19. Hai, Y.; Christianson, D.W. Histone deacetylase 6 structure and molecular basis of catalysis and inhibition. *Nat. Chem. Biol.* **2016**, *12*, 741–747. [[CrossRef](#)]
20. Li, T.; Zhang, C.; Hassan, S.; Liu, X.; Song, F.; Chen, K.; Zhang, W.; Yang, J. Histone deacetylase 6 in cancer. *J. Hematol. Oncol.* **2018**, *11*, 111. [[CrossRef](#)]

21. Dos Santos Passos, C.; Simoes-Pires, C.A.; Carrupt, P.A.; Nurisso, A. Molecular dynamics of zinc-finger ubiquitin binding domains: A comparative study of histone deacetylase 6 and ubiquitin-specific protease 5. *J. Biomol. Struct. Dyn.* **2016**, *34*, 2581–2598. [[CrossRef](#)] [[PubMed](#)]
22. Yang, P.H.; Zhang, L.; Zhang, Y.J.; Zhang, J.; Xu, W.F. HDAC6: Physiological function and its selective inhibitors for cancer treatment. *Drug Discov. Ther.* **2013**, *7*, 233–242. [[CrossRef](#)] [[PubMed](#)]
23. Kaur, S.; Rajoria, P.; Chopra, M. HDAC6: A unique HDAC family member as a cancer target. *Cell. Oncol.* **2022**, *45*, 779–829. [[CrossRef](#)] [[PubMed](#)]
24. Zheng, Y.C.; Kang, H.Q.; Wang, B.; Zhu, Y.Z.; Mamun, M.A.A.; Zhao, L.F.; Nie, H.Q.; Liu, Y.; Zhao, L.J.; Zhang, X.N.; et al. Curriculum vitae of HDAC6 in solid tumors. *Int. J. Biol. Macromol.* **2023**, *230*, 123219. [[CrossRef](#)] [[PubMed](#)]
25. Zhao, Y.; Liang, T.; Hou, X.; Fang, H. Recent Development of Novel HDAC6 Isoform-selective Inhibitors. *Curr. Med. Chem.* **2021**, *28*, 4133–4151. [[CrossRef](#)] [[PubMed](#)]
26. Chen, X.; Chen, X.; Steimbach, R.R.; Wu, T.; Li, H.; Dan, W.; Shi, P.; Cao, C.; Li, D.; Miller, A.K.; et al. Novel 2, 5-diketopiperazine derivatives as potent selective histone deacetylase 6 inhibitors: Rational design, synthesis and antiproliferative activity. *Eur. J. Med. Chem.* **2020**, *187*, 111950. [[CrossRef](#)]
27. Chen, X.; Gong, G.; Chen, X.; Song, R.; Duan, M.; Qiao, R.; Jiao, Y.; Qi, J.; Chen, Y.; Zhu, Y. Design, Synthesis and Biological Evaluation of Novel Benzoylimidazole Derivatives as Raf and Histone Deacetylases Dual Inhibitors. *Chem. Pharm. Bull.* **2019**, *67*, 1116–1122. [[CrossRef](#)] [[PubMed](#)]
28. Peng, J.; Xie, F.; Qin, P.; Liu, Y.; Niu, H.; Sun, J.; Xue, H.; Zhao, Q.; Liu, J.; Wu, J. Recent development of selective inhibitors targeting the HDAC6 as anti-cancer drugs: Structure, function and design. *Bioorg. Chem.* **2023**, *138*, 106622. [[CrossRef](#)]
29. Tavares, M.T.; Shen, S. Recent innovative advances in the discovery of selective HDAC6 inhibitors. *Future Med. Chem.* **2021**, *13*, 1017–1019. [[CrossRef](#)]
30. Zhou, B.; Liu, D.; Tan, Y. Role of HDAC6 and Its Selective Inhibitors in Gastrointestinal Cancer. *Front. Cell Dev. Biol.* **2021**, *9*, 719390. [[CrossRef](#)]
31. Chen, X.; Wang, J.; Zhao, P.; Dang, B.; Liang, T.; Steimbach, R.R.; Miller, A.K.; Liu, J.; Wang, X.; Zhang, T.; et al. Tetrahydro-beta-carboline derivatives as potent histone deacetylase 6 inhibitors with broad-spectrum antiproliferative activity. *Eur. J. Med. Chem.* **2023**, *260*, 115776. [[CrossRef](#)] [[PubMed](#)]
32. Santo, L.; Hideshima, T.; Kung, A.L.; Tseng, J.C.; Tamang, D.; Yang, M.; Jarpe, M.; van Duzer, J.H.; Mazitschek, R.; Ogier, W.C.; et al. Preclinical activity, pharmacodynamic, and pharmacokinetic properties of a selective HDAC6 inhibitor, ACY-1215, in combination with bortezomib in multiple myeloma. *Blood* **2012**, *119*, 2579–2589. [[CrossRef](#)]
33. Huang, P.; Almeciga-Pinto, I.; Jarpe, M.; van Duzer, J.H.; Mazitschek, R.; Yang, M.; Jones, S.S.; Quayle, S.N. Selective HDAC inhibition by ACY-241 enhances the activity of paclitaxel in solid tumor models. *Oncotarget* **2017**, *8*, 2694–2707. [[CrossRef](#)] [[PubMed](#)]
34. Tsimberidou, A.M.; Beer, P.A.; Cartwright, C.A.; Haymaker, C.; Vo, H.H.; Kiany, S.; Cecil, A.R.L.; Dow, J.; Haque, K.; Silva, F.A.; et al. Preclinical Development and First-in-Human Study of KA2507, a Selective and Potent Inhibitor of Histone Deacetylase 6, for Patients with Refractory Solid Tumors. *Clin. Cancer Res.* **2021**, *27*, 3584–3594. [[CrossRef](#)] [[PubMed](#)]
35. Butler, K.V.; Kalin, J.; Brochier, C.; Vistoli, G.; Langley, B.; Kozikowski, A.P. Rational design and simple chemistry yield a superior, neuroprotective HDAC6 inhibitor, tubastatin A. *J. Am. Chem. Soc.* **2010**, *132*, 10842–10846. [[CrossRef](#)] [[PubMed](#)]
36. Blake, J.F.; Gaudino, J.J.; De Meese, J.; Mohr, P.; Chicarelli, M.; Tian, H.; Garrey, R.; Thomas, A.; Siedem, C.S.; Welch, M.B.; et al. Discovery of 5,6,7,8-tetrahydropyrido[3,4-d]pyrimidine inhibitors of Erk2. *Bioorg. Med. Chem. Lett.* **2014**, *24*, 2635–2639. [[CrossRef](#)] [[PubMed](#)]
37. Inoue, S.; Yamane, Y.; Tsukamoto, S.; Murai, N.; Azuma, H.; Nagao, S.; Nishibata, K.; Fukushima, S.; Ichikawa, K.; Nakagawa, T.; et al. Discovery of 5,6,7,8-tetrahydropyrido[3,4-d]pyrimidine derivatives as novel selective Axl inhibitors. *Bioorg. Med. Chem. Lett.* **2021**, *48*, 128247. [[CrossRef](#)] [[PubMed](#)]
38. Delcuve, G.P.; Khan, D.H.; Davie, J.R. Targeting class I histone deacetylases in cancer therapy. *Expert Opin. Ther. Targets* **2013**, *17*, 29–41. [[CrossRef](#)]
39. Lobera, M.; Madauss, K.P.; Pohlhaus, D.T.; Wright, Q.G.; Trocha, M.; Schmidt, D.R.; Baloglu, E.; Trump, R.P.; Head, M.S.; Hofmann, G.A.; et al. Selective class IIa histone deacetylase inhibition via a nonchelating zinc-binding group. *Nat. Chem. Biol.* **2013**, *9*, 319–325. [[CrossRef](#)]
40. Xing, L.; Gong, G.; Chen, X.; Chen, X. Discovery of Indole-Piperazine Hybrid Structures as Potent Selective Class I Histone Deacetylases Inhibitors. *Chem. Pharm. Bull.* **2023**, *71*, 206–212. [[CrossRef](#)]

Disclaimer/Publisher's Note: The statements, opinions and data contained in all publications are solely those of the individual author(s) and contributor(s) and not of MDPI and/or the editor(s). MDPI and/or the editor(s) disclaim responsibility for any injury to people or property resulting from any ideas, methods, instructions or products referred to in the content.